Inorganic Chemistry

Article

Cite This: Inorg. Chem. 2017, 56, 12859-12865

pubs.acs.org/IC

Tailoring Nanocrystalline Metal–Organic Frameworks as Fluorescent Dye Carriers for Bioimaging

UnJin Ryu,[†,§] Jounghyun Yoo,[‡,§] Woosung Kwon,[*,†] and Kyung Min Choi[*,†]

[†]Department of Chemical and Biological Engineering, Sookmyung Women's University, 100 Cheongpa-ro 47 gil, Yongsan-gu, Seoul 04310, Republic of Korea

[‡]Department of Chemical Engineering, Pohang University of Science and Technology (POSTECH), 77 Cheongam-ro, Nam-gu, Pohang 37673, Republic of Korea

Supporting Information

ABSTRACT: Challenges exist in taking advantage of dye molecules for reliable and reproducible molecular probes in biomedical applications. In this study, we show how to utilize the dye molecules for bioimaging within protective carriers of nanocrystalline metal–organic frameworks (nMOFs) particles. Specifically, Resorufin and Rhodamine-6G having different molecular sizes were encapsulated within close-fitting pores of nMOF-801 and nUiO-67 particles, respectively. The resulting nanocrystalline particles have high crystallinity, uniform size, and morphology and preserve enhanced photoluminescence properties with exceptional stabilities in biomedical environment. The samples are further functionalized with a targeting agent and successfully work for fluorescence imaging of FL83B (human hepatocyte cell) and HepG2 (human hepatocellular carcinoma) without cytotoxicity.

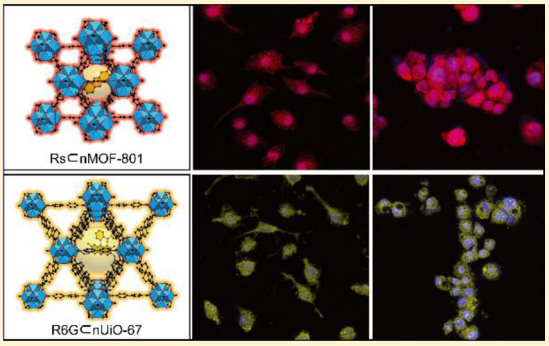

INTRODUCTION

Dye molecules have been widely investigated as fluorophores and offered many advantages because of the diversity with which they can be designed and their absorption and emission range, intensity, fluorescence lifetime, and emission anisotropy are varied.[1−7] Even though dye molecules have been used as fluorescent probes for bioimaging,[8−11] by covalently attaching them on the surface of supports, strategies to utilize dye molecules for reliable and reproducible detection are still challenging. This is because the chemical configurations of dye molecules exposed to the outside are highly affected by the surrounding environment,[12−16] and thus their luminescence properties can be deteriorated or changed in a severe biological environment. We believe that vast opportunities exist for developing methods that selectively encapsulate dye molecules within a close-fitting space inside delivery media while handling them as heterogeneous nanoparticles for biomedical applications. In this study, we encapsulated dye molecules within nanocrystalline metal–organic frameworks (DyeCnMOFs), pore sizes of which are matched with their effective sizes, and then showed that DyeCnMOFs can be successfully used for fluorescence imaging of human cells. Specifically, we chose Resorufin and Rhodamine-6G, which are common dye molecules but are rarely used in the biological environment,[17−20] and confined them within pores of MOF-801[21] and UiO-67[22] during their crystal growth to give nanoparticles[23] of Resorufin-in-nMOF-801 (RsCnMOF-801) and Rhodamine-6G-in-nUiO-67 (R6GCnUiO-67) (Scheme 1). We also confirmed that the dye molecules within nMOFs preserve their fluorescence properties even after 9 days, while pristine ones lose the properties as time goes by in culture media. The surfaces of both DyeCnMOF particles were functionalized and successfully used for reliable and reproducible fluorescence imaging of FL83B (human hepatocyte cell) and HepG2 (human hepatocellular carcinoma) without cytotoxicity.

Many studies involving the luminescence properties of MOFs have been studied by building them with luminescent organic linkers[24−27] or metal ions/clusters,[28−31] diffusing dye molecules into MOFs in a post-treatment procedure,[32−34] or incorporating quantum dots[4,35,36] into the MOFs. This study is the permanent encapsulation of dye molecules during the crystal growth of nMOF particles to utilize the vast library of fluorescent dyes for biomedical applications, which is also different from the release of molecules from MOFs in a drug-delivery system.[37−40] Rhodamine-6G has been encapsulated within bulk MOFs in previous researches[41,42] but not used for bioimaging applications in their nanocrystalline form.

RESULTS AND DISCUSSION

Zirconium(IV)-based nMOFs were chosen because they are thermally and chemically stable in aqueous and ionic conditions, and then two lines of experimentation were carried out that, as we discuss below, reveal the decisive role of size matching between dye molecules and the pores of MOFs (Scheme 1): (1) Resorufin, the effective size of which is 7 Å,

Received: July 2, 2017
Published: October 13, 2017

DOI: 10.1021/acs.inorgchem.7b01684
Inorg. Chem. 2017, 56, 12859−12865

Scheme 1. Schematic Diagrams for the Encapsulation of Resorufin and Rhodamine-6G within nMOFs To Give (a) RsCnMOF-801 and (b) R6GCnUiO-67

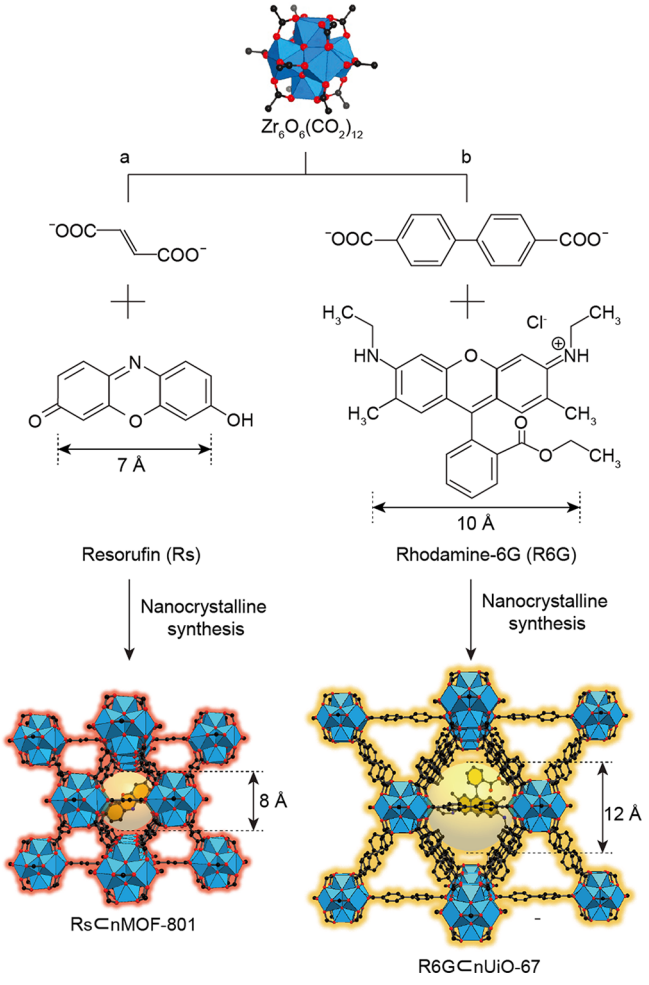

was successfully encapsulated within nMOF-801, having a closely fitted pore size of 8 Å, to give RsCnMOF-801 (Scheme 1a) but washed out from nUiO-67 having bigger pore sizes of 10 and 12 Å; (2) Rhodamine-6G, the effective size of which is 10 Å, was only encapsulated within nUiO-67 to give R6GCnUiO-67 (Scheme 1b). In a typical synthesis, dye molecules were placed in a *N*,*N*-dimethylformamide (DMF) solution mixture containing $ZrCl_4$, organic linkers, trimethylamine (TEA), and acetic acid. TEA was employed to deprotonate carboxylic group at both ends of the organic linkers and make the nucleation reaction dominant to result in nanocrystalline particles. This mixture was placed at 100 °C for 1 day to produce a cloudy and colored solution. The resultant was centrifuged, and the products were collected and washed until no luminescence was detected in the supernatant DMF, which was followed by further solvent exchange using methanol for 3 days and drying under vacuum (see the Experimental Section for synthesis details). All materials were characterized by powder X-ray diffraction (PXRD), nitrogen gas adsorption, scanning electron microscopy (SEM), transmission electron microscopy (TEM), and photoluminescence (PL) spectroscopy. These techniques were used to characterize the crystallinity, permanent porosity, morphology, luminescence properties, and stabilities of DyeCnMOFs.

For each of the RsCnMOF-801 and R6GCnUiO-67 samples, high crystallinity is evident from the sharp diffraction lines of their PXRD patterns (Figure 1a), and the coincidence of the

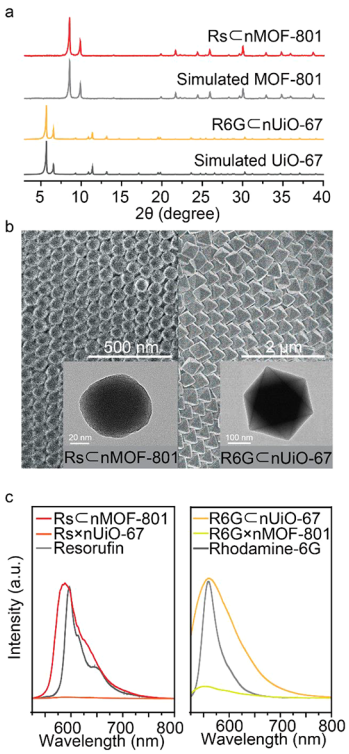

Figure 1. Characterization and PL properties of DyeCnMOFs. (a) PXRD patterns of DyeCnMOFs in comparison with the pattern of the corresponding MOFs. (b) SEM images of RsCnMOF-801 and R6GCnUiO-67. The insets are TEM images of each. (c) PL spectra for Resorufin, Rhodamine-6G, R6GxnUiO-67, RsxnUiO-67, RsCnMOF-801, and R6GCnUiO-67.

diffraction lines matching those of the simulated pattern clearly indicates preservation of the original MOF-801 and UiO-67 structure arrangement[21−23] upon the introduction of dye molecules into their nanocrystalline form. RsCnMOF-801 and R6GCnUiO-67 were all synthesized as single and monocrystalline nanoparticles because this effects their affinity, selectivity, and accessibility to the biological system. Representative SEM images in Figure 1b show the great uniformity of RsCnMOF-801 (ca. 100 nm) and R6GCnUiO-67 (ca. 400 nm) and identical octahedral geometry of the particles. The size and shape of each particle were also confirmed by TEM, as shown in the insets of Figure 1b.

PL spectra were measured to prove the existence of dye molecules in DyeCnMOF particles. Dried samples of RsCnMOF-801 and R6GCnUiO-67 were measured using PL spectroscopy. Figure 1c shows that the PL spectra of both samples are consistent with those of the dye molecules, which reveals that the dye molecules preserve their luminescent properties upon encapsulation within nMOFs. Each nMOF sample without dyes shows no PL in the same wavelength region (Figure S1). Because the organic dyes could be sensitive to the acidity and the MOF synthesis solution has a pH 2.5 value, we tested the fluorescence of dyes in different pH conditions to check whether they are stable in a MOF synthesis process (Figures S2−S5). This revealed that Resorufin is protonated at acidic conditions (pH <4) but recovers its

DOI: 10.1021/acs.inorgchem.7b01684
Inorg. Chem. 2017, 56, 12859−12865

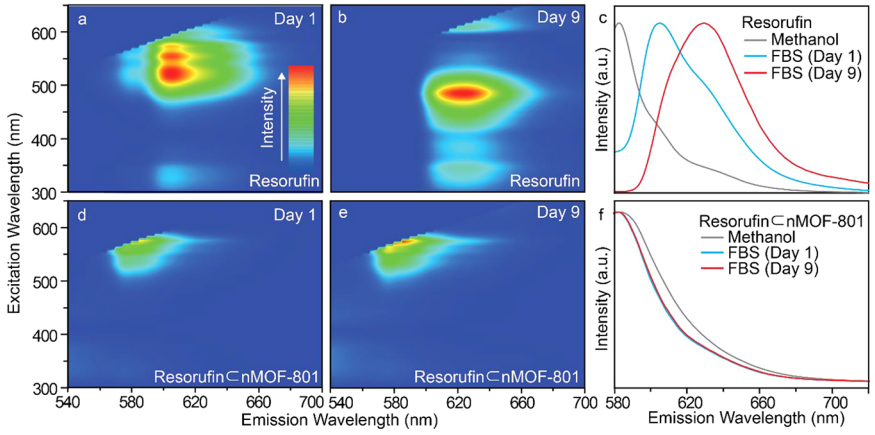

Figure 2. PL contour maps of (a and b) Resorufin and (d and e) Rs⊂nMOF-801 excited at 570 nm in FBS kept for (a and d) 1 day and (b and e) 9 days. PL spectra of (c) Resorufin and (f) Rs⊂nMOF-801 excited at 570 nm in methanol and FBS recorded on a daily basis for 9 days.

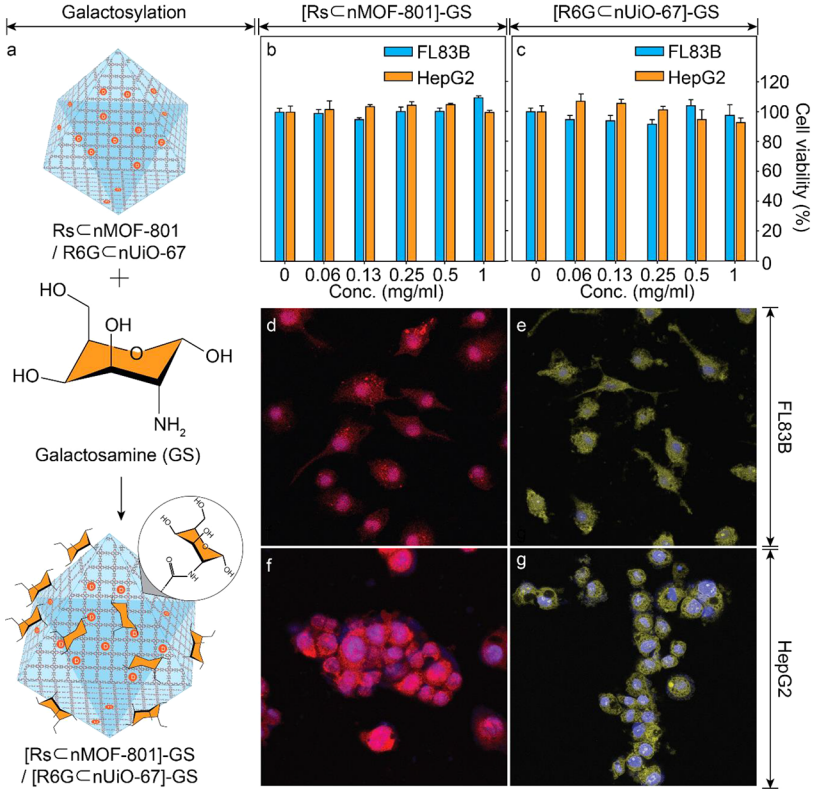

Figure 3. Surface functionalization, human cell imaging, and cytotoxicity of Dye⊂nMOFs. (a) Schematic diagrams for the surface functionalization of Rs⊂nMOF-801 and R6G⊂nUiO-67 with galactosamine to give [Rs⊂nMOF-801]-GS and [R6G⊂nUiO-67]-GS. Tests for the cytotoxicity for (b) [Rs⊂nMOF-801]-GS and (c) [R6G⊂nUiO-67]-GS. Images of (d and e) FL83B and (f and g) HepG2 using (d and f) [Rs⊂nMOF-801]-GS and (e and g) [R6G⊂nUiO-67]-GS.

original form and fluorescence in the washing process after MOF synthesis, while Rhodamine-6G remains unchanged throughout the entire synthetic process.

Because it is also possible that dye molecules are attached to the outside of the nMOF particles or jammed in defect sites regardless of the pore sizes of the MOFs,[43] we decided to test whether the nMOF samples with switched dye molecules are still working for PL. The nMOF-801 and nUiO-67 particles were synthesized in the presence of Rhodamine-6G and Resorufin to give R6G×nMOF-801 and Rs×nUiO-67, respectively, and washed with DMF and methanol until no dye molecules were found in the washing solvents, which was exactly the same procedure for Rs⊂nMOF-801 and R6G⊂nUiO-67. In this procedure, Rhodamine-6G should not be introduced within the pores of MOF-801 in the synthetic process, while Resorufin should be swept away from the pores of UiO-67 during the washing process. These R6G×nMOF-801 and Rs×nUiO-67 samples show no PL in the wavelength range in which the dye molecules work (Figure 1c), which clearly indicates that the dye molecules were size-selectively encapsulated within the pores of MOFs to give Rs⊂nMOF-801 and R6G⊂nUiO-67.

The amount of dye molecules encapsulated within Dye⊂nMOFs was calculated by the PL intensity of the

DOI: 10.1021/acs.inorgchem.7b01684
Inorg. Chem. 2017, 56, 12859−12865

DyeCnMOFs compared with that of the dye molecules (Figure S8 and Tables S1 and S2). The PL intensity of the dye molecules was plotted against their concentrations in methanol (Figure S8), and the lines were extrapolated to the PL intensity of the DyeCnMOF samples under the assumption that the PL intensity is linearly proportional to the amount of dye molecules at a very low concentration. Extrapolation of the PL intensity gives the numbers of Resorufin and Rhodamine-6G in 1 mg of RsCnMOF-801 and R6GCnUiO-67 as 1.91×10^{15} and 2.80×10^{12}, respectively. The mole percentages of dye molecules for RsCnMOF-801 and R6GCnUiO-67 are 4.3×10^{-2} and 8.7×10^{-5} mol %, respectively, so that the estimated occupancies of the dyes in the pores are 1.7×10^{-1} and 4.0×10^{-4}%, respectively. It is confirmed by nitrogen adsorption isotherm measurements (Figure S9) that the DyeCnMOFs have extra pores while showing enough fluorescence, which indicates that such extra pores can potentially be used to carry therapeutic molecules or other functional materials.

The photostabilities of the dyes and DyeCnMOFs were also tested under continuous irradiation of 365 nm UV light (Figures S10 and S11). After 24 h of irradiation, RsCnMOF-801 maintained 78% PL intensity, while Resorufin showed 6% compared to the original intensity of the unexposed one. These results show that the photostability of the Resorufin dye was greatly enhanced by encapsulation within MOF-801. In the case of Rhodamine-6G, its high intrinsic photostability was also maintained within R6GCnUiO-67, and there was no perceivable shift in the PL peak position or degradation in the PL intensity after 24 h of irradiation.

The stability of the dyes and DyeCnMOFs against the biological environment was tested in fetal bovine serum (FBS), which is a serum supplement commonly used in biological research. The dyes and DyeCnMOFs were dispersed in FBS for up to 9 days, and their PL spectra were recorded on a daily basis. When the solvent was changed from methanol to FBS, the PL spectra of Resorufin were red-shifted by ca. 20 nm (from 582 nm in methanol to 605 nm in FBS), as shown in Figure S12a. Then, the PL spectra of Resorufin were gradually aggravated during 9 days (Figures 2a−c and S12a), while RsCnMOF-801 preserved its original PL spectrum in FBS even after 9 days (Figures 2d−f and S12c). Interestingly, the PL spectra of RsCnMOF-801 were identical in both methanol and FBS (Figure 2f), unlike the Resorufin molecule (Figure 2c), which presumably indicates that the dye molecules within nMOF-801 generally remain unexposed to FBS. In the case of Rhodamine-6G in FBS, its original stability was also preserved in R6GCnUiO-67 (Figure S12b,d). The stability of DyeCnMOFs was also tested in phosphate-buffered saline (PBS), which proved that both DyeCMOFs preserved their original PL spectrum in PBS even after 9 days without dye leaching (Figure S13). These results imply that dye molecules can be protected from biological environments by encapsulating them within the nMOF pores; therefore, DyeCnMOF can realize reliable and reproducible fluorescence detection in biological systems.

Galactosylation of RsCnMOF-801 and R6GCnUiO-67 gave [RsCnMOF-801]-GS and [R6GCnUiO-67]-GS through the amidation reaction between the carboxyl function groups on the nMOF surface and the amine group of galactosamine (Figure 3a). Galactosylation increases the cell biocompatibility and membrane permeability of nanoparticles by enhancing recognition and binding between galactose residues and the liver-specific asialoglycoprotein receptor in the plasma membranes of liver cells.[44,45] For galactosylation, DyeCnMOFs in distilled water were mixed with an excess amount of galactosamine, and then 1-ethyl-3-[3-(dimethylamino)propyl]-carbodiimide (EDC) was used as a carboxyl activating agent to initiate the reaction (see the Experimental Section for detailed experimental procedures). Galactosylation of RsCnMOF-801 and R6GCnUiO-67 has been identified by attenuated total reflection Fourier transform infrared (ATR-FTIR) spectroscopy, PXRD, elemental analysis (EA), and thermogravimetric analysis (TGA; Figures S14−S16). In the ATR-FTIR spectra of [RsCnMOF-801]-GS (Figure S14a), symmetric vibration of the carboxylate group (1392 cm^{-1}) peak of RsCnMOF-801 decreased, while C−O stretching of the secondary (1100 cm^{-1}) and primary (1045 cm^{-1}) alcohol peaks newly appeared by galactosylation. In the case of [R6GCnUiO-67]-GS (Figure S14b), asymmetric vibration of the carboxylate group (1584 cm^{-1}) and symmetric vibration of the carboxylate group (1401 cm^{-1}) peaks decreased, while an amide II band (C−N stretching vibrations in combination with N−H bending; 1652 cm^{-1}), C−O stretching of the secondary alcohol (1101 cm^{-1}), and C−O stretching of the primary alcohol (1049 cm^{-1}) developed by galactosylation. The PXRD results indicate that [DyeCnMOF]-GS samples preserve the original nMOF structure arrangement after galactosylation (Figure S15). Peak broadening observed for both samples indicates that a large amount of galactosamine is attached on the surface of DyeCnMOF. From EA, [RsCnMOF-801]-GS and [R6GCnUiO-67]-GS have 11.3 and 25.1 wt % galactosamine, which corresponds to the results from TGA (Figure S16). These results confirm that RsCnMOF-801 and R6GCnUiO-67 were successfully galactosylated by an amidation reaction. Tetrazolium-based colorimetric (MTT) assay was then carried out for testing the cytotoxicity of [RsCnMOF-801]-GS and [R6GCnUiO-67]-GS in FL83B and HepG2 cells. The MTT solution was added to the FL83B and HepG2 cells both treated with [RsCnMOF-801]-GS and [R6GCnUiO-67]-GS, and the cell viability was measured by the optical density of MTT−formazan at 540 nm on an absorbance microplate reader (see methods for detailed experimental procedures). Parts b and c of Figure 3 show the relative cell viability of the FL83B and HepG2 cells after treatment with 0.06−1 mg/mL concentration of [RsCnMOF-801]-GS and [R6GCnUiO-67]-GS for 24 h. The cytotoxicity of [DyeCnMOF]-GS was almost negligible in both the FL83B and HepG2 cells because their cell viability only fluctuated in the range of 90−110% at different concentrations. Overall, the results demonstrate the biocompatibility of [DyeCnMOF-801]-GS and their potency as safe bioimaging agents.

Parts d−g of Figure 3 show the confocal laser scanning microscopic images of the FL83B and HepG2 cells after incubation at 37 °C for 2 h in the presence of [RsCnMOF-801]-GS and [R6GCnUiO-67]-GS. As shown in Figure 3d,f, the FL83B and HepG2 cells treated with [RsCnMOF-801]-GS showed strong red fluorescence from Resorufin dyes inside nMOF-801. Similarly, FL83B and HepG2 cells treated with [R6GCnUiO-67]-GS (Figure 3e,g) also showed strong yellow-green fluorescence, which corresponds to the emission of Rhodamine-6G. When RsCnMOF-801 and R6GCnUiO-67 (both without galactosylation) were used for cell imaging in the same procedure, the FL83B and HepG2 cells were not visualized, but their nuclei were stained in blue for cell identification (Figure S17). In vitro bioimaging results proved that both [RsCnMOF-801]-GS and [R6GCnUiO-67]-GS were effectively taken up by the FL83B and HepG2 cells and

DOI: 10.1021/acs.inorgchem.7b01684
Inorg. Chem. 2017, 56, 12859−12865

demonstrated the use of nMOFs as a protective carrier of molecular probes for bioimaging.

CONCLUSIONS

We show how molecular dyes that were a challenge to use in the biomedical environment are encapsulated within pores of nMOFs and successfully utilized for reliable and reproducible fluorescence bioimaging of human cells. Resorufin and Rhodamine-6G having different molecular sizes are encapsulated within close-fitting pores of nMOF-801 and nUiO-67 particles, respectively. The resulting nMOFs have high crystallinity, uniform size, and morphology and preserve enhanced PL properties with exceptional stabilities in the biomedical environment. These samples are functionalized with a targeting agent and successfully work for fluorescence imaging of FL83B (human hepatocyte cell) and HepG2 (human hepatocellular carcinoma) without cytotoxicity. We expect that this will open vast opportunities to utilize the library of molecular dyes in biomedical applications.

EXPERIMENTAL SECTION

Synthesis of nMOFs. The ligand parts [fumaric acid (18 mg, 0.15 mmol) for nMOF-801 and biphenyl-4,4′-dicarboxylic acid (19.4 mg, 0.08 mmol) for nUiO-67] were dissolved with TEA (0.03 mL) in DMF (5 mL). $ZrCl_4$ (1:1 molar ratio of $ZrCl_4$/ligand) was also prepared in DMF (5 mL) with acetic acid (0.69 mL for nMOF-801 and 1.38 mL for nUiO-67), separately. The two solutions were combined in a 20 mL glass vial and sealed before placement in a 100 °C oven for 12 h. The white suspensions thus produced were collected and washed with DMF using a centrifuge (8000 rpm for 10 min) and a sonicator and then sequentially immersed in methanol for three 24 h periods. Finally, the samples were activated by removing the solvent under vacuum at room temperature.

Synthesis of Dyes⊂nMOFs. Dyes were initially dissolved in DMF at concentrations of 0.48 and 0.21 mg/mL for Resorufin and Rhodamine-6G, respectively, and used as a solvent for Dyes⊂nMOFs preparation. The ligand parts [fumaric acid (18 mg, 0.15 mmol) for Dye⊂nMOF-801 and biphenyl-4,4′-dicarboxylic acid (19.4 mg, 0.08 mmol) for Dye⊂nUiO-67] were dissolved with TEA (0.03 mL) in a Dye-DMF solution (5 mL). $ZrCl_4$ (1:1 molar ratio of $ZrCl_4$/ligand) was also prepared in Dye-DMF (5 mL) with acetic acid (0.69 mL for nMOF-801 and 1.38 mL for nUiO-67), separately. The two solutions were combined in a 20 mL glass vial and sealed before placement in a 100 °C oven for 12 h. The colored suspensions were collected and washed with DMF using a centrifuge (8000 rpm for 10 min) and a sonicator and then sequentially immersed in methanol for three 24 h periods. Finally, the samples were activated by removing the solvent under vacuum at room temperature.

Characterizations. The PXRD spectra were obtained by a Rigaku X-ray diffractometer (Smartlab, Cu Kα radiation) at 1200 W (40 kV, 30 mA). The scanning condition was a 4°/min scan rate from 3° to 40° with a silicon holder. The morphology and surface of the MOFs were verified by a field emission scanning electron microscope (JEM-7600F, JEOL). The powder sample was dissolved in methanol and dropped directly onto the holder. For TEM observation, samples were first dispersed in methanol by sonication and dropped onto a TEM grid. TEM was carried out at 200 kV using a JEOL JEM-2100F microscope. The PL spectra of the powder sample were obtained by a high-resolution micro low-temperature PL system (LabRAM HR UV/vis/NIR PL). The entire scan range was 525−800 nm, and the excitation wavelength was 514 nm. The PL spectra of the solution sample were obtained by a Jasco FP-8500 fluorometer with QS-grade quartz cuvettes (111-QS, Hellma Analytics). Gas adsorption analysis was performed on a BELSORP-max automatic volumetric gas adsorption analyzer. Samples were prepared and measured after evacuation at 100 °C for 12 h. ATR-FTIR spectroscopy was performed using a Nicolet iS50 FTIR spectrometer (Thermo-Scientific). EA of the powder sample was performed on an EA112/FLASH2000 analyzer. It was obtained through three replicate experiments. TGA was obtained by a TGA4000 analyzer at a rising temperature of 5 °C/min.

Surface Functionalization of Dye⊂nMOFs with Galactosamine. Dye⊂nMOF was dissolved in distilled water (5 mg/mL) and mixed with a 5-fold weight excess of D-(+)-galactosamine hydrochloride. The pH of the solution was adjusted to 4.8 by the addition of 0.1 N HCl and then mixed with a 20-fold molar excess of EDC. During the reaction, the pH of the solution was consistently maintained at 4.8 and stirred. After 2 h, the pH of the solution was raised to 7.0 by the addition of NaOH (0.1 N) to terminate the reaction. The resulting solution was dialyzed against a NaCl aqueous solution (100 mM) for 2 days, 25% ethanol for 1 day, and distilled water for 2 days. [Dye⊂nMOF]-GSs were obtained by freeze-drying.

Cell Culture. In this study, the FL83B human liver epithelial cell line and the HepG2 human liver cell line were obtained by a Korean Cell Link Bank. The FL83B and HepG2 cells were cultured in Dulbecco's modified Eagle medium (DMEM) supplemented with FBS (10 vol %) and antibiotics (1 wt %), respectively. Each cell was seeded on each well of a 96-well cell culture plate at a density of 10^4 cells/well and cultured in a humidified 5% CO_2 cell culture incubator at 37 °C before use.

Cell Treatment and Cytotoxicity Tests of [Dye⊂nMOFs]-GS. The cytotoxicity of [Rs⊂nMOF-801]-GS and [R6G⊂nUiO-67]-GS was assessed by MTT assay, respectively. Fresh DMEM containing [Rs⊂nMOF-801]-GS and [R6G⊂nUiO-67]-GS with increasing [Rs⊂nMOF-801]-GS and [R6G⊂nUiO-67]-GS concentrations was added to each well and incubated for 24 h, respectively. Then, a MTT solution (100 μL, 0.5 mg/mL) in DMEM was added to each well and incubated at 37 °C for 2 h. The medium of each well was aspirated and treated with dimethyl sulfoxide (50 μL) to dissolve the formazan crystal. The optical density was measured at 540 nm with an absorbance microplate reader (EMax microplate reader, Bucher Biotec AG, Basel, Switzerland).

In Vitro Bioimaging of [Dye⊂nMOFs]-GS. The FL83B and HepG2 cells were seeded on an eight-chamber glass slide at a density of 2×10^4 cells/well and cultured in DMEM supplemented with FBS (10 vol %) and antibiotics (1 wt %) in a humidified 5% CO_2 cell culture incubator at 37 °C for 24 h. The culture medium was replaced with FBS-free DMEM. Then, [Rs⊂nMOF-801]-GSs and [R6G⊂nUiO-67]-GSs (1 mg/mL) in serum-free DMEM (300 μL) were added to the wells of the culture slides, respectively. The cells were incubated for 2 h, washed with PBS, fixed with paraformaldehyde (4 wt %) in PBS, washed again with PBS twice, and mounted by a VECTASHIELD antifade mounting medium with 4′,6-diamidine-2′-phenylindole dihydrochloride (DAPI). The sample-treated cells were observed with a confocal laser scanning microscope (Leica TCS SP5u MP SMD FLIM) at a magnification of 250×. The internalized [Rs⊂nMOF-801]-GSs or [R6G⊂nUiO-67]-GSs in the cytoplasm were excited with an argon laser at 561 nm. An LD405 laser at 405 nm was used to visualize DAPI.

ASSOCIATED CONTENT

Supporting Information

The Supporting Information is available free of charge on the ACS Publications website at DOI: 10.1021/acs.inorgchem.7b01684.

Materials and methods, supporting characterization of MOF, Dye⊂*n*MOF, and Dye×*n*MOF, and biological experiments (PDF)

AUTHOR INFORMATION

Corresponding Authors

*E-mail: wkwon@sookmyung.ac.kr.
*E-mail: kmchoi@sookmyung.ac.kr.

DOI: 10.1021/acs.inorgchem.7b01684
Inorg. Chem. 2017, 56, 12859−12865

ORCID

Kyung Min Choi: 0000-0001-7181-902X

Author Contributions

[§]These authors contributed equally.

Author Contributions

U.R. and K.M.C. initiated the project and planned the experiments. They also prepared and analyzed the samples of RsCnMOF-801 and R6GCnUiO-67. J.Y. and W.K. analyzed the fluorescence properties of RsCnMOF-801 and R6CnUiO-67 and conducted biological experiments. All of the authors discussed the results and wrote the manuscript.

Notes

The authors declare no competing financial interest.

■ ACKNOWLEDGMENTS

The research was supported by Basic Science Research Programs of the National Research Foundation of Korea (NRF; Grants 2016R1C1B1010781 and 2016R1C1B1011830) and partially by the Nano Material Technology Development Program through the NRF funded by the Ministry of Science, ICT, and Future Planning (Grant 2009-0082580). We especially thank Hyemin Kim (POSTECH) for her technical help in the biological experiments.

■ REFERENCES

(1) Waring, D. R.; Hallas, G. *The chemistry and application of dyes*; Plenum Press: New York, 1990.

(2) Soper, S. A.; Nutter, H. L.; Keller, R. A.; Davis, L. M.; Shera, E. B. The photophysical constants of several fluorescent dyes pertaining to ultrasensitive fluorescence spectroscopy. *Photochem. Photobiol.* **1993**, *57*, 972−977.

(3) Umezawa, K.; Nakamura, Y.; Makino, H.; Citterio, D.; Suzuki, K. Bright, color-tunable fluorescent dyes in the visible− near-infrared region. *J. Am. Chem. Soc.* **2008**, *130*, 1550−1551.

(4) Resch-Genger, U.; Grabolle, M.; Cavaliere-Jaricot, S.; Nitschke, R.; Nann, T. Quantum dots versus organic dyes as fluorescent labels. *Nat. Methods* **2008**, *5*, 763−775.

(5) Hawe, A.; Sutter, M.; Jiskoot, W. Extrinsic fluorescent dyes as tools for protein characterization. *Pharm. Res.* **2008**, *25*, 1487−1499.

(6) Li, X.; Gao, X.; Shi, W.; Ma, H. Design strategies for water-soluble small molecular chromogenic and fluorogenic probes. *Chem. Rev.* **2014**, *114*, 590−659.

(7) Luo, S.; Zhang, E.; Su, Y.; Cheng, T.; Shi, C. A review of NIR dyes in cancer targeting and imaging. *Biomaterials* **2011**, *32*, 7127−7138.

(8) Escobedo, J. O.; Rusin, O.; Lim, S.; Strongin, R. M. NIR dyes for bioimaging applications. *Curr. Opin. Chem. Biol.* **2010**, *14*, 64−70.

(9) Chan, J.; Dodani, S. C.; Chang, C. Reaction-based small-molecule fluorescent probes for chemoselective bioimaging. *Nat. Chem.* **2012**, *4*, 973−984.

(10) Yuan, L.; Lin, W.; Zheng, K.; He, L.; Huang, W. Far-red to near infrared analyte-responsive fluorescent probes based on organic fluorophore platforms for fluorescence imaging. *Chem. Soc. Rev.* **2013**, *42*, 622−661.

(11) Guo, Z.; Park, S.; Yoon, J.; Shin, I. Recent progress in the development of near-infrared fluorescent probes for bioimaging applications. *Chem. Soc. Rev.* **2014**, *43*, 16−29.

(12) Ince, N. H. Critical" effect of hydrogen peroxide in photochemical dye degradation. *Water Res.* **1999**, *33*, 1080−1084.

(13) Torimura, M.; Kurata, S.; Yamada, K.; Yokomaku, T.; Kamagata, Y.; Kanagawa, T.; Kurane, R. Fluorescence-quenching phenomenon by photoinduced electron transfer between a fluorescent dye and a nucleotide base. *Anal. Sci.* **2001**, *17*, 155−160.

(14) O'neill, C.; Lopez, A.; Esteves, S.; Hawkes, F. R.; Hawkes, D. L.; Wilcox, S. Azo-dye degradation in an anaerobic-aerobic treatment system operating on simulated textile effluent. *Appl. Microbiol. Biotechnol.* **2000**, *53*, 249−254.

(15) Vogelsang, J.; Kasper, R.; Steinhauer, C.; Person, B.; Heilemann, M.; Sauer, M.; Tinnefeld, P. A reducing and oxidizing system minimizes photobleaching and blinking of fluorescent dyes. *Angew. Chem., Int. Ed.* **2008**, *47*, 5465−5469.

(16) Rauf, M. A.; Ashraf, S. S. Fundamental principles and application of heterogeneous photocatalytic degradation of dyes in solution. *Chem. Eng. J.* **2009**, *151*, 10−18.

(17) Rose, M. J.; Fry, N. L.; Marlow, R.; Hinck, L.; Mascharak, P. K. Sensitization of ruthenium nitrosyls to visible light via direct coordination of the dye resorufin: trackable NO donors for light-triggered NO delivery to cellular targets. *J. Am. Chem. Soc.* **2008**, *130*, 8834−8846.

(18) Choi, M. G.; Hwang, J.; Eor, S.; Chang, S.-K. Chromogenic and fluorogenic signaling of sulfite by selective deprotection of resorufin levulinate. *Org. Lett.* **2010**, *12*, 5624−5627.

(19) Michaels, A. M.; Nirmal, M.; Brus, L. E. Surface enhanced Raman spectroscopy of individual rhodamine 6G molecules on large Ag nanocrystals. *J. Am. Chem. Soc.* **1999**, *121*, 9932−9939.

(20) Kneipp, K.; Wang, Y.; Dasari, R. R.; Feld, M. S. Approach to single molecule detection using surface-enhanced resonance Raman scattering (SERRS): A study using Rhodamine 6G on colloidal silver. *Appl. Spectrosc.* **1995**, *49*, 780−784.

(21) Wißmann, G.; Schaate, A.; Lilienthal, S.; Bremer, I.; Schneider, A. M.; Behrens, P. Modulated synthesis of Zr-fumarate MOF. *Microporous Mesoporous Mater.* **2012**, *152*, 64−70.

(22) Cavka, J. H.; Jakobsen, S.; Olsbye, U.; Guillou, N.; Lamberti, C.; Bordiga, S.; Lillerud, K. P. A new zirconium inorganic building brick forming metal organic frameworks with exceptional stability. *J. Am. Chem. Soc.* **2008**, *130*, 13850−13851.

(23) Choi, K. M.; Jeong, H. M.; Park, J. H.; Zhang, Y.-B.; Kang, J. K.; Yaghi, O. M. Supercapacitors of nanocrystalline metal−organic frameworks. *ACS Nano* **2014**, *8*, 7451−7457.

(24) Wei, Z.; Gu, Z.-Y.; Arvapally, R. K.; Chen, Y.-P.; McDougald, R. N., Jr; Ivy, J. F.; Yakovenko, A. A.; Feng, D.; Omary, M. A.; Zhou, H.-C. Rigidifying fluorescent linkers by metal−organic framework formation for fluorescence blue shift and quantum yield enhancement. *J. Am. Chem. Soc.* **2014**, *136*, 8269−8276.

(25) Cui, Y.; Yue, Y.; Qian, G.; Chen, B. Luminescent functional metal−organic frameworks. *Chem. Rev.* **2012**, *112*, 1126−1162.

(26) Liu, D.; Huxford, R. C.; Lin, W. Phosphorescent nanoscale coordination polymers as contrast agents for optical imaging. *Angew. Chem., Int. Ed.* **2011**, *50*, 3696−3700.

(27) Li, Y.-A.; Zhao, C.-W.; Zhu, N.-X.; Liu, Q.-K.; Chen, G.-J.; Liu, J.-B.; Zhao, X.-D.; Ma, J.-P.; Zhang, S.; Dong, Y.-B. Nanoscale UiO-MOF-based luminescent sensors for highly selective detection of cysteine and glutathione and their application in bioimaging. *Chem. Commun.* **2015**, *51*, 17672−17675.

(28) Foucault-Collet, A.; Gogick, K. A.; White, K. A.; Villette, S.; Pallier, A.; Collet, G.; Kieda, C.; Li, T.; Geib, S. J.; Rosi, N. L.; Petoud, S. Lanthanide near infrared imaging in living cells with Yb3+ nano metal organic frameworks. *Proc. Natl. Acad. Sci. U. S. A.* **2013**, *110*, 17199−17204.

(29) Kundu, T.; Mitra, S.; Díaz Díaz, D.; Banerjee, R. Gadolinium (III) Based Porous Luminescent Metal−Organic Frameworks for Bimodal Imaging. *ChemPlusChem* **2016**, *81*, 728−732.

(30) Miller, S. E.; Teplensky, M. H.; Moghadam, P. Z.; Fairen-Jimenez, D. Metal-organic frameworks as biosensors for luminescence-based detection and imaging. *Interface Focus* **2016**, *6*, 20160027.

(31) Liu, D.; Lu, K.; Poon, C.; Lin, W. Metal−organic frameworks as sensory materials and imaging agents. *Inorg. Chem.* **2014**, *53*, 1916−1924.

(32) Wuttke, S.; Braig, S.; Preiß, T.; Zimpel, A.; Sicklinger, J.; Bellomo, C.; Rädler, J. O.; Vollmar, A. M.; Bein, T. MOF nanoparticles coated by lipid bilayers and their uptake by cancer cells. *Chem. Commun.* **2015**, *51*, 15752−15755.

(33) Dong, M.-J.; Zhao, M.; Ou, S.; Zou, C.; Wu, C.-D. A luminescent dye@ MOF platform: emission fingerprint relationships

DOI: 10.1021/acs.inorgchem.7b01684
Inorg. Chem. 2017, 56, 12859−12865

of volatile organic molecules. *Angew. Chem., Int. Ed.* **2014**, *53*, 1575−1579.
(34) Hu, X.-L.; Qin, C.; Wang, X.-L.; Shao, K.-Z.; Su, Z.-M. A luminescent dye@ MOF as a dual-emitting platform for sensing explosives. *Chem. Commun.* **2015**, *51*, 17521−17524.
(35) Buso, D.; Jasieniak, J.; Lay, M. D. H.; Schiavuta, P.; Scopece, P.; Laird, J.; Amenitsch, H.; Hill, A. J.; Falcaro, P. Highly luminescent metal−organic frameworks through quantum dot doping. *Small* **2012**, *8*, 80−88.
(36) Zhao, D.; Wan, X.; Song, H.; Hao, L.; Su, Y.; Lv, Y. Metal−organic frameworks (MOFs) combined with ZnO quantum dots as a fluorescent sensing platform for phosphate. *Sens. Actuators, B* **2014**, *197*, 50−57.
(37) Horcajada, P.; Chalati, T.; Serre, C.; Gillet, B.; Sebrie, C.; Baati, T.; Eubank, J. F.; Heurtaux, D.; Clayette, P.; Kreuz, C.; Chang, J.-S.; Hwang, Y. K.; Marsaud, V.; Bories, P.-N.; Cynober, L.; Gil, S.; Férey, G.; Couvreur, P.; Gref, R. Porous metal-organic-framework nanoscale carriers as a potential platform for drug delivery and imaging. *Nat. Mater.* **2010**, *9*, 172−178.
(38) Deng, K.; Hou, Z.; Li, X.; Li, C.; Zhang, Y.; Deng, X.; Cheng, Z.; Lin, J. Aptamer-mediated up-conversion core/MOF shell nanocomposites for targeted drug delivery and cell imaging. *Sci. Rep.* **2015**, *5*, 7851.
(39) Agostoni, V.; Horcajada, P.; Noiray, M.; Malanga, M.; Aykac, A.; Jicsinszky, L.; Vargas-Berenguel, A.; Semiramoth, N.; Daoud-Mahammed, S.; Nicolas, V.; Martineau, C.; Taulelle, F.; Vigneron, J.; Etcheberry, A.; Serre, C.; Gref, R. A "green" strategy to construct non-covalent, stable and bioactive coatings on porous MOF nanoparticles. *Sci. Rep.* **2015**, *5*, 7925.
(40) Li, Y.-A.; Zhao, X.-D.; Yin, H.-P.; Chen, G.-J.; Yang, S.; Dong, Y.-B. A drug-loaded nanoscale metal−organic framework with a tumor targeting agent for highly effective hepatoma therapy. *Chem. Commun.* **2016**, *52*, 14113−14116.
(41) Fang, Q.-R.; Zhu, G.-S.; Jin, Z.; Ji, Y.-Y.; Ye, J.-W.; Xue, M.; Yang, H.; Wang, Y.; Qiu, S.-L. Mesoporous metal-organic framework with rare etb topology for hydrogen storage and dye assembly. *Angew. Chem., Int. Ed.* **2007**, *46*, 6638−6642.
(42) Choi, K. M.; Jeon, H. J.; Kang, J. K.; Yaghi, O. M. Heterogeneity within order in crystals of a porous metal−organic framework. *J. Am. Chem. Soc.* **2011**, *133*, 11920−11923.
(43) Trickett, C. A.; Gagnon, K. J.; Lee, S.; Gándara, F.; Bürgi, H.-B.; Yaghi, O. M. Definitive molecular level characterization of defects in UiO-66 crystals. *Angew. Chem., Int. Ed.* **2015**, *54*, 11162−11167.
(44) Kim, E.-M.; Jeong, H.-J.; Kim, S.-L.; Sohn, M.-H.; Nah, J.-W.; Bom, H.-S.; Park, I.-K.; Cho, C.-S. Asialoglycoprotein-receptor-targeted hepatocyte imaging using ^{99m}Tc galactosylated chitosan. *Nucl. Med. Biol.* **2006**, *33*, 529−534.
(45) Hama, Y.; Urano, Y.; Koyama, Y.; Choyke, P. L.; Kobayashi, H. D-galactose receptor-targeted in vivo spectral fluorescence imaging of peritoneal metastasis using galactosamin-conjugated serum albumin-rhodamine green. *J. Biomed. Opt.* **2007**, *12*, 051501.

DOI: 10.1021/acs.inorgchem.7b01684
Inorg. Chem. 2017, 56, 12859−12865